Design and Analysis of a Hyperelastic Pneumatic Honeycomb Network Made of Ecoflex 00-35

S. Unseld[1*], A. Baumer[1], R. Goller[1], T. Koch[2], I. Kuehne[3] and A. Frey[1]
[1]University of Applied Sciences, Augsburg, Germany, [2]Comsol Multiphysics GmbH, Göttingen, Germany, [3]Heilbronn University, Kuenzelsau, Germany
*Corresponding author: An der Hochschule 1, 86161 Augsburg, Germany, simon.unseld@hs-augsburg.de

Abstract: Using the *Solid Mechanics* application mode a model is setup to investigate the expansion behavior of a hyper-elastic pneumatic honeycomb network (PHN). A contact model is used to investigate the expanding behavior of the PHN near planar surfaces. Based on the simulation results the nonlinear expanding behavior of a PHN made of Ecoflex 00-35 can be achieved for different configurations.

The results suggest, that these PHN can be used as dynamic sealant for different applications, as the incompressibility of the Ecoflex 00-35 and the high expansion at a low internal pressure allow a high degree of flexibility for sealing a wide variety of geometries.

Keywords: hyperelasticity, Mooney Rivlin, pneumatic honeycomb network

1. Introduction

Pneumatic honeycomb networks are biologically inspired soft robots that can be controlled by air pressure. Soft robotics is a subgroup of robotics, whose soft, highly elastic materials are used to avoid the coupling of rigid materials. Their evenly distributed deformation enables hyper-redundant configurations, providing high dexterity in uneven environments [1]. These networks can be composed of an outer layer with reinforcements to prevent circumferential loads and consequently the expansion of the material in unwanted directions, and the honeycomb network between these layers (cf. **Fig. 1**).

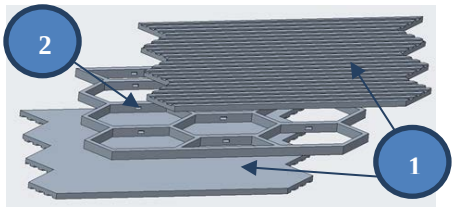

Fig. 1: Components of a PHN: (1) outer skin with reinforcements, (2) honeycomb network

By simulating the pneumatic honeycomb network, the expansion behaviour of the structure as a function of selected parameters is to be carried out by means of a parametric study.

In this paper only the network itself is considered. Under the assumption that air chambers exert a uniform pressure on the network depending on their internal pressure, these chambers can be neglected in the structural modeling and thus the computing time can be significantly reduced. The structural modelling is done in the X-Y-plane with a two-dimensional structure.

2. Determination of material characteristics

In order to simulate hyperelastic materials, the non-linear stress-strain relationship needs to be determined through different tests and implemented with different theoretical models. For the simulation of the PHN, the material silicone (Ecoflex 00-35) is used. The material characteristics are determined by uniaxial tensile tests. The code number 00-35 indicates the hardness according to Shore-A. In the tempered state, Ecoflex 00-35 has an elongation at break up to 900% at a Young's modulus of 7.5 N/mm^2 and a tear strength of 6.78 N/mm^2. [2]

2.1 Hyper-elastic materials model

Hyper-elastic materials like Ecoflex 00-35 show large elastic deformations at small loads and have a non-linear relation between stress and strain. With the removal of the load, hyper-elastic materials can regain their original shape despite high deformations. Particularly rubber is almost completely incompressible. Thus, the shape of material changes when large loads are applied, but the total volume is approximately constant at all times.

In the finite element analysis, the non-linear stress-strain behaviour is characterized by

theoretical models that approximate the real material behaviour with geometric nonlinearity using the strain energy density function W_s, described in [3] and [4].

The second Piola-Kirchhoff stress tensor for hyperelastic material is defined as:

$$S = 2\frac{\partial W_s}{\partial C} \tag{1}$$

where:

W_s: strain energy density
C: eigenvalues of the Right Cauchy-Green tensor with $\mathbf{F^T F}$

For isotropic hyper-elasticity, the formula mentioned above can be extended to:

$$S = 2\left[\left(\frac{\partial W_s}{\partial I_1} + \frac{\partial W_s}{\partial I_2}\right) I - \frac{\partial W_s}{\partial I_2} C + I_3 \frac{\partial W_s}{\partial I_3} C^{-1}\right] \tag{2}$$

with $I_{1,2,3}$ being the invariants of the Right Cauchy-Green tensor

To obtain the invariants, the Right Cauchy-Green tensor needs to be written in its spectral form:

$$C = \sum_{k=1}^{3} {\lambda^2}_k \widehat{N}_k \otimes \widehat{N}_k \tag{3}$$

where:

λ^2_k: eigenvalues oft the Right Cauchy Green tensor
N_k: corresponding principal referential directions

Combining (2) and (3) yields:

$$C = \sum_{k=1}^{3} \frac{1}{\lambda_k} \frac{\partial W_s}{\partial \lambda_k} \widehat{N}_k \otimes \widehat{N}_k \tag{4}$$

The eigenvalues $\lambda_{1\text{-}3}$ can be obtained through various tests. The most common types are the uniaxial and biaxial tension and compression test, as well as the pure shear test. In this paper, the uniaxial tension test for specified tensile specimen is performed. Assuming complete incompressibility (J=1), the eigenvalues of the right Cauchy-Green tensor can be determined according to M. Mooney as follows:

$$\lambda_1 = \lambda \qquad \lambda_2 = \lambda^{-1/2} \qquad \lambda_3 = \lambda^{-1/2} \tag{5}$$

with λ being the principled stretch.

Assuming incompressibility for the uniaxial tension/compression test, the isochoric invariants of the right Cauchy-Green tensor can be calculated to:

$$I_{1_{uni}} = \left(\lambda^2 + \frac{2}{\lambda}\right) \quad I_{2_{uni}} = \left(2\lambda + \frac{1}{\lambda^2}\right) \tag{6}$$

2.2 Uniaxial tensile tests

The tensile strength of Ecoflex 00-35 is tested using the universal testing machine from Hegewald & Peschke with a 5kN load cell. The tensile tests are carried out according to DIN [5]. Due to its relatively low viscosity, it is not necessary to degas the casted tensile specimens if the mould is poured slowly and from high distances in order to break small entrapped air bubbles. However, the elasticity of the individual specimen can vary, since the mechanical properties differ depending on small air inclusions inside the structure. Tensile specimens that have not been properly cast or degassed can take less load, which means that the individual tensile tests differ from each other. **Fig. 2** shows a degassed and a non-degassed test specimen with a magnification of x150 (left) and x50 (right).

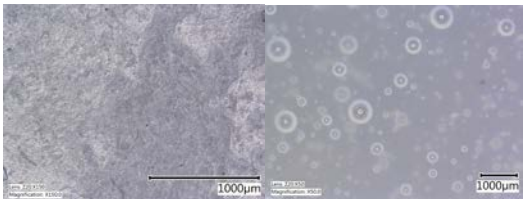

Fig. 2: Microscope images of a degassed specimen (left, x150) and non-degassed specimen (right, x50)

Due to their low stiffness, the tensile specimens must be provided with a certain amount of pre-tension when clamped, otherwise it is difficult to fix them. The position of the clamping device is set to zero after the specimen has been clamped successfully. The pre-

tensioning is set to the minimum tensioning of the tensile test.

The experiment is performed for five specimens. **Fig. 3** shows the result of the test in terms of the maximum displaceable distance of the testing machine. The test speed, selected according to DIN 53504, is 200mm/min. As already noted, untreated tensile specimens contain air entrapments which reduce the mechanical resistance of the tensile specimens. A direct comparison between untreated and degassed samples can be taken from **Fig. 3**.

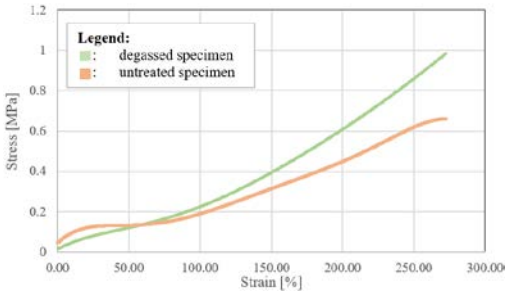

Fig. 3: Stress-strain curve for Ecoflex 00-35

2.3 Implementation in COMSOL-Multiphysics using the Money-Rivlin-5-Parameter model

In this paper, the 5-parameter Mooney-Rivlin model is used. It is valid up to a maximum elongation of 200-250%. The Mooney-Rivlin model is a polynomial approximation [6-9]. It can be described as:

$$W_s = \sum_{i+j=1}^{N} C_{ij}(I_1 - 3)^i (I_2 - 3)^j + \\ + \sum_{i=1}^{N} \frac{1}{D_i}(J-1)^{2i} \quad (7)$$

where:

W_s: strain energy density
C_{ij}: model specific constant
$I_{1,2}$: volumetric invariant (zero if incompressible)
D_i: compressibility factor
J: Jacobian or derivation matrix

The Mooney-Rivlin 5-parameter model corresponds to the polynomial approximation at N=2 considering certain assumptions. This results in the following relationship regarding the Mooney-Rivlin model:

$$W_{s1} = C_{10}(\bar{I}_1 - 3) + C_{01}(\bar{I}_2 - 3) + \\ C_{11}(\bar{I}_1 - 3)(\bar{I}_2 - 3)$$
$$W_{s2} = C_{20}(\bar{I}_1 - 3) + C_{02}(\bar{I}_1 - 3) + \frac{1}{2}K(J_{el} - 1)^2 \quad (8)$$
$$W_s = W_{s1} + W_{s2}$$

A curve fit in Matlab is performed, in which the model parameters can be approximated through experimental data [10]. **Fig. 4** shows the measured data compared to the approximated data used for the Mooney-Rivlin 5-parameter model.

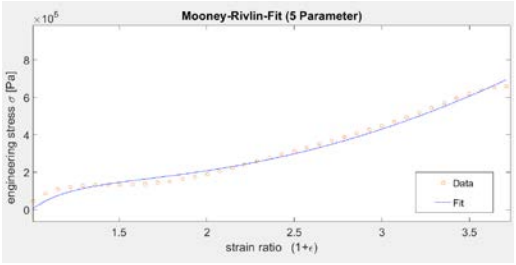

Fig. 4: Curve-fit for the measured stress-strain data

It can be noted that the determined graph is remarkably accurate with respect to the actual measurements. Therefore, the simulation parameters only deviate slightly from reality. The material parameters determined from this curve fit are transferred to COMSOL as fixed numerical parameters. The occurring stresses and corresponding displacements can be calculated by partial derivation of the strain energy density:

$$\sigma = \frac{\partial W_s}{\partial \lambda} \quad (8)$$

where:

σ: stress
λ: principled stretch
W_s: strain energy density

The compression module D1 must be specified in addition to the model parameters C01-C20 in order to obtain almost complete incompressibility and quadratic volumetric strain energy. A first linear approximation can be described as:

$$D_1 = \frac{3(1-2\nu)}{2(\nu+1)(C_{10}+C_{01})} \quad (9)$$

where:

E: Youngs Modulus
v: Poisson's ratio

Commonly used for silicone is a poisson's ratio of 0.495. The determined model parameters do not represent the actual material properties up to an elongation at break of 900%. However, due to the 5-parameter Mooney-Rivlin model, the generated material should not be stressed beyond an elongation up to 250%. The material defined in COMSOL therefore has the appropriate prerequisites. When considering the calculation for higher strains, this must be taken into account, but cannot be considered otherwise in this paper due to the maximum travel distance of the test device.

3. System modelling

The honeycomb structure is modelled in steady-state solid mechanics. The system is modelled within a two-dimensional domain in order to save computing time and to achieve good convergence behaviour. As this simulation deals with a planar and not a circular structure, no stresses caused by the shrinking of the material in circumferential direction when expanding downwards are present. This is neglected in this simulation, as the convergence behaviour of hyper-elastic materials can often be difficult to obtain.

3.1 Parametrization and geometry

For this study, different dimensions for the web length L_i, the thickness d and the pressures $p_{i,m}$, $p_{i,l}$ and $p_{i,r}$ shall be investigated. **Fig. 5** shows the structure of a single cell with the implemented parameters.

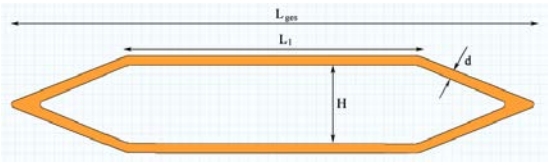

Fig. 5: Geometry of a single cell

The overall geometry shown in **Fig. 5** is modelled as a function of the parameters**.** The radii, which should prevent the formation of singularities at corners, are a fraction of the structure thickness d. As a result, it can be guaranteed that the entire geometry is adapted to the dimensions in case of subsequent modifications of the parameters. This is illustrated in **Tab 1.** Here, the construction points X1-X3 as well as Y1-Y2 are used to define the inner contour of a single cell.

Tab. 1: Section of the defined parameters for the generation of a single cell

Construction Point	Coordinate
X1	$(L_{ges}-L_1)/2$
X2	$L_1+(L_{ges}-L_1)/2$
X3	L_{ges}
Y1	H
Y2	H/2

This cell is then duplicated using an array to create a 3x3 honeycomb network. **Fig. 6** shows the overall geometry for the parameters L_i*=10mm,* L_{ges}*=55mm, d=1mm, H=10mm.*

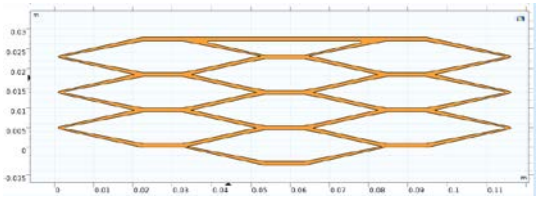

Fig. 6: Entire geometry of the simulated pneumatic network

Since the pressure in the chambers is also varied as a parameter for investigations, the use of symmetry is deliberately avoided.

3.2 Meshing

The simulation of hyper-elastic materials requires a fine mesh. Since very high strains and displacements can be expected, the elements must be selected in such a way, that even in case of very large distortions compared to the original mesh, the mesh quality is sufficient to achieve a suitably accurate result. As the entire geometry only consists of very thin cell connectors in the 2D range, an acceptable computing time can be achieved even with very fine meshes. The

meshing is done manually, with the maximum and minimum element size corresponding to a fraction of the web thickness *d*, in order to maintain a consistently fine and structured mesh during parameter variation of the thickness. In this way, convergence problems caused by changed mesh qualities can be minimised to a large extent. **Fig. 7** shows the mesh for the parameters L_i*=40mm* and *t=2mm.* The structure of this mesh only changes insignificantly when varying the thickness.

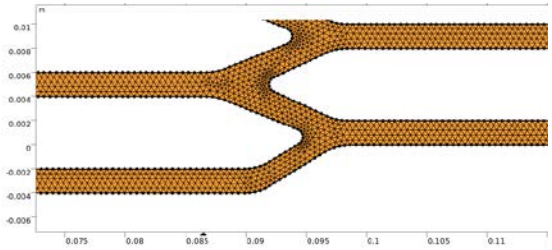

Fig. 7: Meshing of the structure with triangles

A mesh refinement is carried out on the inner radii, as the biggest deformations can be expected here due to the bending of the cells. Simple mesh studies show that triangular elements show a better convergence behaviour at high deformations, therefore, the generation of rectangular elements is avoided in this study.

In order to evaluate the accuracy of the simulations depending on the mesh quality, a mesh refinement is performed. In this case, the predefined element size parameters are chosen. **Fig. 8** shows the difference in element size between the coarse, normal and extremely fine option for the parameters L_i*=40mm, d=1mm.*

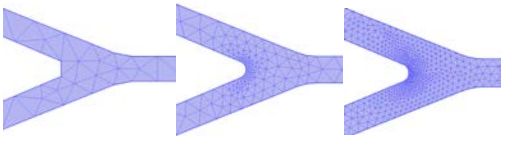

Fig. 8: Difference in element size between the predefined element size options coarse (left), normal (middle) and extremely fine (right)

For comparison, the maximum von Mises stress is evaluated for each predefined element size. The results of the mesh refinement study can be seen in **Fig. 9**.

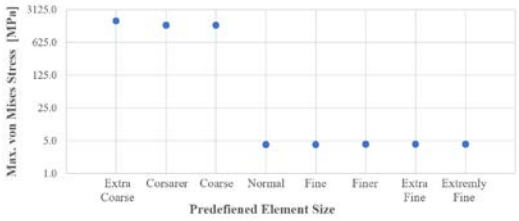

Fig. 9: Results of the mesh refinement study for the maximum von Mises stress

The results state that the influence of the element size regarding the results can be neglected for a predefined mesh size of 'normal' or better. The percentual deviation in the maximum stress between 'normal' and 'extremly fine' amounts to 1%. A chosen element size larger than the thickness *d* shows a high degree of inaccuracy. Considering the defined dependency of the element size regarding the cell-parameter *d*, the predefined size 'normal' equals a maximum element size of *d/2*. For this study, a maximum element size of *d/4*, and a minimum size of *d/6* is chosen to ensure good convergence for each parameter variation.

3.3 Assignment of physical properties

The internal pressures $p_{i,left}$, $p_{i,middle}$ and $p_{i,right}$ applied to the corresponding inner surfaces. $p_{i,left}$ affects the three left cells, $p_{i,middle}$ the middle cells and $p_{i,right}$ the right cells. At the top of the geometry, the network is defined as rigid constraint. The whole geometry is defined as hyper-elastic material. For this purpose, the Mooney-Rivlin 5-parameter model is used with an almost incompressible material with quadratic volumetric strain energy. The material constants correspond to the values determined in section **2.2**.

To investigate the contact behavior of the PHN with a planar surface, three contact areas of the PHN are declared destinations, and a planar surface is declared source (cf. **Fig. 10**).

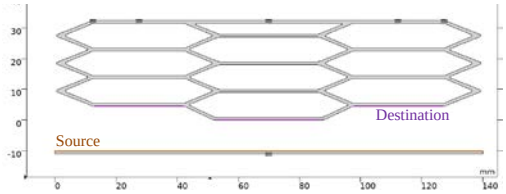

Fig. 10: Contact definition

The penalty method is used. In addition, the ramp factor *para* is introduced, which is used by auxiliary sweep to gradually increase the pressure in the cells. The internal pressures p_{i_l}, p_{i_r} and p_{i_m} are multiplied by the factor *para* (cf. **Fig. 11**).

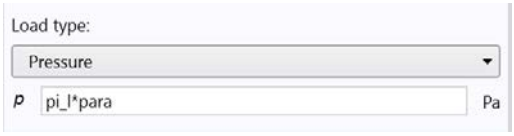

Fig. 11: Definition of the pressure in dependence of the ramp factor

3.4 Parametric and auxiliary sweep

The variation of the parameters is done by a parametric sweep in COMSOL. This allows for different parameter combinations to be simulated and displayed in the desired configurations. Thus, it is possible to investigate different modifications of the network for its maximum expansion and stresses. For this study, a total of fifteen different configurations will be calculated. Five configurations are calculated for varied cell-connector length L_i (referred to as L1 in **Fig. 11**), the material thickness d is calculated in three configurations. **Fig. 11** shows the parametric sweep with the selected parameter combinations.

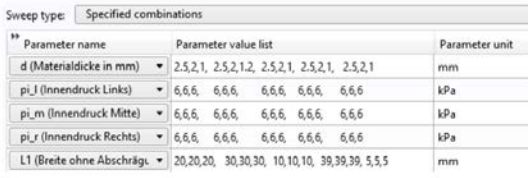

Fig. 11: Selected Variations for Parametric Sweep

The contact simulation is performed for the parameter combination *Li=30mm, d=1mm*. The auxiliary sweep is used to gradually increase the pressure within the cells using a ramp factor called *para* until full contact with the plane is established (cf. **Fig. 12**).

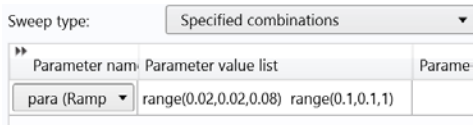

Fig. 12: Specified auxiliary sweep for the parameter combination L_i*=30mm, d=1mm*

The ramp factor *para* starts with 0, which corresponds to a pressure of 0 within the cells. The Continuation Method will be used by default, which uses the solution from the previously solved step as the initial condition for the next step. This improves the convergence of the contact simulation significantly.

4. Validation

The validation of the simulation is done by comparing a prototype with L1=30mm and d=1mm. The simulation result from **Fig. 14** provides a maximum displacement of 29.49mm, whereas the prototype in **Fig. 13** provides a displacement of 27mm for an internal pressure of 6kPa.

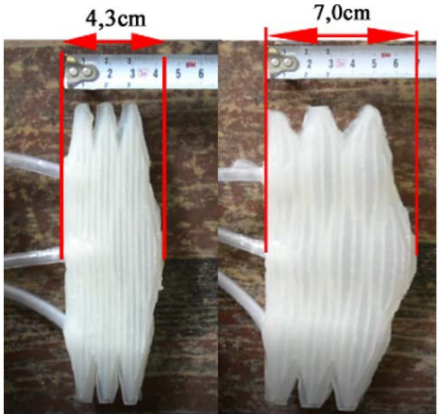

Fig. 13: Expansion of the prototype at 6kPa

The pressure is adjusted using pressure sensors and solenoid valves. The simulation results thus represent a good approximation to the experiment.

5. Results

Fig. 14 shows the results of the parameter constellation L_i=30mm, d=1mm/2mm, H=10mm as well as L_i=40mm/10mm, d=1mm, H=10mm. Based on the simulation data, the crucial parameter for the change in expansion behaviour is the cell-connector length L_i. The thickness also has a significant influence on the expansion behaviour of a cell.

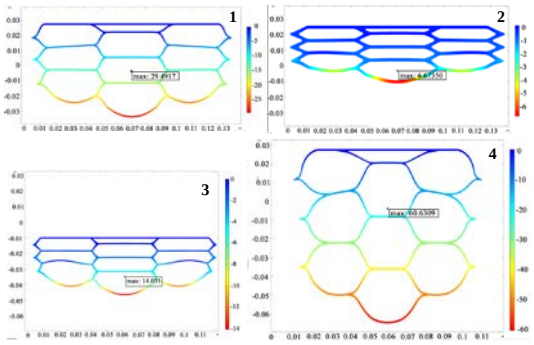

Fig. 14: Variation of the thickness (1mm, 1 – 2mm, 2) and variation of the cell connector length L_i (40mm, 3 – 10mm, 4)

The initial height of all configurations is 30mm. This results in an elongation of 200% for **Fig. 14, (3)**. All measured values are thus within the validity range of the 5-parameter Mooney-Rivlin model. The simulated data can be gathered in a three-dimensional diagram to show the trends for achieving maximum expansion properties (see **Fig. 15**). It becomes clear that both the cell connector length L_i and the thickness d have a significant influence on the expansion properties.

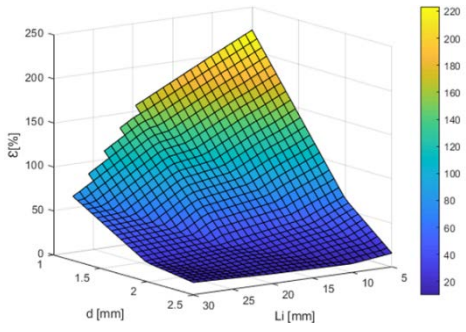

Fig. 15: 3D plot of the material thickness d and the cell connector length L_i as a function of the expansion ε (Matlab R2019)

Another important aspect of the simulation is the analysis of the stresses that occur in the material. Using the diagram in **Fig. 15**, the constellation with the highest total strain and thus the greatest expansion can be determined. This constellation is found at L_i=5mm, d=1mm, H=10mm. The corresponding stresses can be taken from **Fig. 16**.

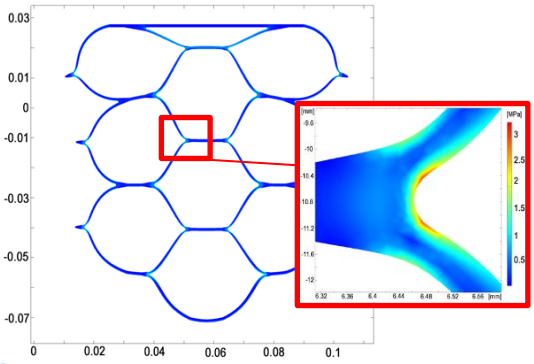

Fig. 16: Stress due to expansion of the honeycomb structure

The highest stress can be observed at the connection areas between the individual cells. Due to the strong bending of the cells, these areas experience a tension of up to 3.89N/mm^2, which makes tearing of the material most likely at this point. The maximum tensile strength of the material is 6.78 N/mm^2, thus a tearing of the structure is unlikely if sufficient degassing before curing is achieved. The result of the contact simulation is shown in **Fig. 17**.

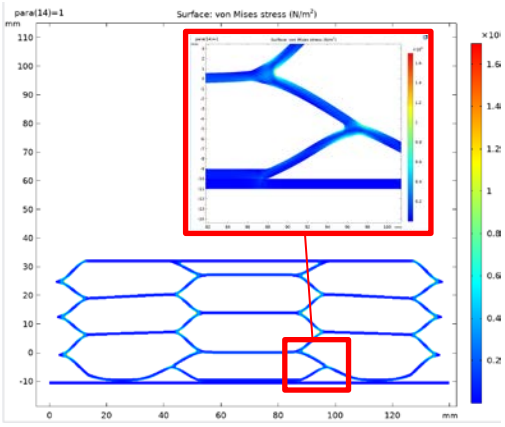

Fig. 17: Contact simulation of the PHN with a planar surface

Fig. 16 shows that the individual cell connector absorb almost no load, similar to the contact simulation in **Fig. 17**, even though the inner pressure tries to compress the cell connectors. One of the reasons for this is the nearly complete incompressibility of the material. When loads are applied, the material tends to change its shape in order to reduce the stresses. This behaviour is desired in this application.

A height influence study will not be performed in this work, as this parameter shall be designed as small as possible for space saving applications. In summary, based on the generated simulation data, a clear relationship between maximum elongation and the geometric quantities length and thickness can be identified. Therefore, it is possible to create a honeycomb network by using minimal amounts of material, thus achieving high expansions with minimal load. The data also provide information about the resulting stresses and the contact behaviour of the structure. In addition, the maximum potential of the structure can be shown and different elastic materials can be easily investigated by determining the material properties through tensile tests in order to find the optimal material for this structure.

6. Literature

[1] Triverdi, D., Rahn, C. D., Kier W. M., Walker, I. D., *Soft robotics: Biological inspiration, state of the art, and future research*. Applied Bionics and Biomechanics, 5(3), 2008, 99-117.

[2] s.n.: *KauPo, ECOFLEX 00-35*, last accessed 17.12.19, 18:00 MEZ

[3] Hamza, H., Alwan, H., *Hyperelastic Constitutive Modeling of Rubber and Rubber-Like Materials under Finite Strain.* Eng.& Tech. Journal, 28 (13), 2010 2560–2575.

[4] Muhr, A. H., *Modeling the stress–strain behavior of rubber*. Rubber chemistry and technology, 78(3*), 2010,* 391–425.

[5] DIN 53504:2017-03, *Prüfung von Kautschuk und Elastomeren -Bestimmung von Reißfestigkeit, Zugfestigkeit, Reißdehnung und Spannungswerten im Zugversuch*

[6] Rivlin, R. S., *Large elastic deformations of isotropic materials. IV. Further developments of the general theory*, Philosophical Transactions of the Royal Society of London. Series A, Mathematical and Physical Sciences, 241(835), 1948, 379–397.

[7] Boulanger, P. and Hayes, M. A., *Finite amplitude waves in Mooney–Rivlin and Hadamard materials*, in *Topics in Finite Elasticity*, ed. M. A Hayes and G. Soccomandi, International Center for Mechanical Sciences, 2001, 131-167.

[8] Mooney, M., *A theory of large elastic deformation*, Journal of Applied Physics, 11(9), 1940, 582–592.

[9] Boyce, M.C., Arruda, E.M., *Constitutive models of rubber elasticity: A Review*, Rubber Chemistry and Technology, 73, 2000, 504-523.

[10] [..] N. Philippin, A. Schreivogel, I. Kuehne & J. Kostelnik: *Electronics of a new dimension - Potentials of stretchable foil systems for development of interactive microimplants*. EBL - Elektronische Baugruppen und Leiterplatten, Fellbach, 68-73, 2020.